CO2 conversion in a photocatalytic continuous membrane reactor — **Source link** ⤴

M. Sellaro, Marianna Bellardita, Adele Brunetti, Enrica Fontananova ...+3 more authors

Institutions: University of Calabria, University of Palermo

Topics: Membrane reactor, Membrane and Methanol

Related papers:

- Photocatalytic CO2 Reduction in Gas-Solid Regime in the Presence of Bare, SiO2 Supported or Cu-Loaded TiO2 Samples

- CO2 to Liquid Fuels: Photocatalytic Conversion in a Continuous Membrane Reactor

- Improving photoreduction of CO2 with homogeneously dispersed nanoscale TiO2 catalysts

- Review of material design and reactor engineering on TiO2 photocatalysis for CO2 reduction

- Effect of TiO2 particle size on the photocatalytic reduction of CO2

Share this paper: 📘 🐦 💼 ✉

View more about this paper here: https://typeset.io/papers/co2-conversion-in-a-photocatalytic-continuous-membrane-1zqhb0a1xa

CO$_2$ conversion in a photocatalytic continuous membrane reactor

M. Sellaro,[a] M. Bellardita,[b] A. Brunetti,[a] E. Fontananova,[a] L. Palmisano,[b] E. Drioli[ac] and G. Barbieri*[a]

The reduction of CO$_2$ with water by using photocatalysts is one of the most promising new methods for achieving CO$_2$ conversion to valuable hydrocarbons such as methanol (MeOH). In this work, prepared TiO$_2$–Nafion™-based membranes were used in a photocatalytic membrane reactor, operated in continuous mode, for converting CO$_2$ to methanol. By using the membrane with the best TiO$_2$ distribution, a MeOH flow rate/TiO$_2$ weight of 45 μmol (g$_{catalyst}$ h)$^{-1}$ was measured when operating at 2 bar of feed pressure. This value is higher than those reported in most of the literature data to date. Moreover, methanol production is considered as a relevant advance over the existing literature results which mostly propose CH$_4$ as the reaction product.

Introduction

One of the main causes of global climate change is greenhouse gas emission with *ca.* 36 Gton of CO$_2$ emitted per year both by natural sources, including decomposition, and by human sources such as the burning of fossil fuels (coal, oil and natural gas), cement production, deforestation, *etc.*[1] Today, many efforts have led to the concretization of capture processes able to separate CO$_2$ from the rest of the emitted gaseous streams with a targeted level of purity, together with a minimal energy penalty.[2] Some cases have achieved a good level of success; however, the main hurdle remains the final destination of these huge CO$_2$ streams. On the one hand, storage may be the most likely option, but on the other hand, the identification of new environmentally improved routes and methods may enable the reduction of emissions. Moreover, the obtaining of new sustainable energy sources is a key challenge, which would have a significant environmental impact. To this purpose, new greener technologies have been studied and developed, especially to convert CO$_2$ into useful chemical species and fuels.[3,4] Actually, converting CO$_2$ to valuable hydrocarbons seems to be one of the most recent advances in Carbon Capture and Utilization (CCU), being one of the best solutions to both global warming and energy requirements. The reduction of CO$_2$ with water to fuels by using photocatalysts is one of the most promising methods to be investigated, as it represents a green process and an attractive route from economic and environmental points of view. CO$_2$ can be converted by irradiating it with UV light at room temperature and ambient pressure and thus solar energy can be directly transformed and stored as chemical energy.[5,6]

Therefore, the photoreduction of CO$_2$ to chemicals, such as methane and methanol, is of great interest. In particular, the main goal is the production of methanol, as it can be easily transported, stored and used as a gasoline-additive, as well as transformed to other useful chemicals by means of classic technologies.[5]

Inoue *et al.*[7] first reported the production of formic acid, formaldehyde and trace amounts of methanol from the reduction of CO$_2$ with water by irradiation of aqueous suspensions of semiconductor powders such as TiO$_2$, whereas the photocatalytic production of methane from CO$_2$ was first reported by Hemminger *et al.*[8]

Nevertheless, this technology presents some difficulties related to non-effective catalysts, low yield and poor selectivity. From a thermodynamic perspective, CO$_2$ conversion with water into methanol and oxygen (eqn (1)) is endergonic, the Gibbs molar free energy being 698.7 kJ mol^{-1} at 298 K.

$$CO_2 + 2H_2O \underset{}{\overset{h\nu}{\rightleftharpoons}} CH_3OH + \frac{3}{2}O_2 \qquad (1)$$
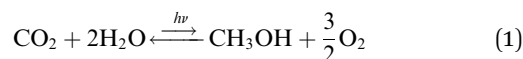
In order to improve the efficiency of the reaction, many research efforts have been directed to the development of several new types of photocatalysts.[9]

Among all the applied photocatalysts, TiO$_2$ has been shown to be one of the most used materials for the photocatalytic conversion of CO$_2$ into fuels, owing to its chemical inertness, lack of photocorrosion, stability against photoirradiation,

[a]Institute on Membrane Technology (ITM-CNR), National Research Council, c/o the University of Calabria, Cubo 17C, Via Pietro Bucci, 87036 Rende CS, Italy. E-mail: g.barbieri@itm.cnr.it

[b]Department of Energy, Information Engineering and Mathematical Models (DEIM), University of Palermo, Viale delle Scienze, 90128 Palermo PA, Italy

[c]Department of Environmental and Chemical Engineering, University of Calabria, Cubo 44A, Via Pietro Bucci, 87036 Rende CS, Italy

suitable optical and electronic qualities, low cost, commercial availability, and non-toxic nature.[10]

TiO_2 anatase and rutile band gaps are located at about 3.2 eV and 3.0 eV, respectively and the best photocatalytic efficiency can be obtained using anatase with a small admixture of rutile (approximately 75% anatase and 25% rutile).[10,11]

However, in addition to the nature of the photocatalyst to be used, one should consider that the photocatalytic conversion of CO_2 is a surface reaction involving two important stages: (1) CO_2 adsorption to the catalyst surface; and (2) CO_2 decomposition under UV irradiation in the presence of reductants. Therefore, the mass transfer rate of CO_2, and the catalyst surface area are two other important parameters which must be controlled to improve the photocatalytic efficiency. As a consequence, catalyst configuration during the photochemical reaction is of high concern to increase the yield of products.

The immobilization of the catalyst into polymeric membrane supports and, thus the use of a membrane reactor for this type of reaction, can be an interesting and valid solution to adopt. The use of a membrane reactor offers several advantages such as a better exposition of catalyst to UV light to carry out the reaction, the tailoring of contact between reactants and catalyst, the reduction of catalyst aggregate formation, an easier recovery of the catalyst which can be simply reused, and a better control of fluid-dynamics. Moreover, polymeric membranes are easily handled and offer lower costs with respect to other inorganic supports.

Up to now, many studies have developed photocatalytic membranes with TiO_2 deposited on or entrapped in them.[12–17] They have been used especially for water purification or wastewater treatment in advanced oxidation processes, for reduction reactions,[18,19] and also for pilot-plant experiments as in the case of the PHOTOPERM® process for the degradation of phenol and other organic compounds.[20–22] Leong et al.[23] have recently reviewed the types of membranes used as supports and related photocatalytic membrane preparation and characterization, focusing on the application of TiO_2 photocatalytic membranes for the removal of pollutant contaminated water.

TiO_2 can be successfully supported on perfluorinated ionomer membranes, taking advantage of the superior chemical stability and the optical qualities of the membranes themselves. Nafion™ is the most studied perfluorinated material and several studies have been performed on the use of Nafion™ thin films or membranes as supports for metal or semiconductor particles.[24,25] It was demonstrated that Nafion™ can be useful not only as a support on which to fix semiconductor particles but also as a stabilizing agent for semiconductor microcrystalline colloids.[26] Nafion™ is constituted from an extremely hydrophobic perfluorinated hydrocarbon backbone and several side-chains with fixed sulfonic end groups able to interact with charged/polar species via electrostatic interactions and hydrogen bonds.[27] In this way the polymer conjugates offer high stability under quite harsh conditions, including UV irradiation. Nafion™ has a high affinity for charged/polar catalysts, as well as offering a functional microstructured environment that can have a positive influence on the transition states and reaction kinetics for the formation of polar products.[28] Moreover, as is

also reported in the literature, no change of the band gap is expected when TiO_2 is incorporated in the Nafion™.[19]

Miyoshi et al.[26] prepared TiO_2 microcrystallites in Nafion™, adding an alcoholic Nafion™ solution to TiO_2 colloids. The obtained TiO_2/Nafion™ in wet form was then used for photo-decomposition of acetic acid into CH_4 and CO_2. In many cases, TiO_2 has been incorporated in Nafion™ commercial membranes by soaking them in a solution of Ti-precursor and then treating the Ti-loaded films to obtain the formation of TiO_2 particles.[24,29,30] As regards CO_2 conversion, in 1997, Premkumar and Ramaraj[31] prepared metal porphyrin and phthalocyanine adsorbed Nafion™ membranes to be used for the photocatalytic reduction of CO_2 to formic acid. More recently, Pathak et al.[32] immobilized TiO_2 nanoparticles in the porous cavities of commercial Nafion™ membranes, soaking them in an iso-propanol solution of $Ti(OC_3H_7)_4$ and then immersing the obtained films in boiling water to form TiO_2 nanoparticles by hydrolysis. They found out that the homogeneous dispersion of the photocatalyst in Nafion™ thin films allowed the photore-duction of CO_2 under optically homogeneous reaction conditions, with consequent improved conversion. In a typical experiment, they filled an optical cell, containing the photo-catalytic film, with supercritical CO_2 to a final pressure of 138 bar (2000 psi). After irradiation through a water filter for 5 h, the production of formic acid, together with methanol and acetic acid was observed. Subsequently, Pathak et al.[33] performed other catalytic tests using TiO_2-loaded Nafion™ membranes coated with silver metal via photolysis in which the major reaction product was methanol.

In this work, photocatalytic Nafion™ membranes were prepared by immobilizing bare TiO_2, previously synthesized from a $TiCl_4$ precursor, into the polymeric matrix. Both the catalyst powder and then the photocatalytic membranes obtained were characterized by means of different techniques. Finally, the membranes were tested in order to verify their catalytic efficiency for CO_2 photoreduction with water to obtain methanol under UV-Vis irradiation in a continuous reactor. To the best of our knowledge, this work is the first example of a photocatalytic reactor operated in continuous mode for CO_2 photoreduction using dense mixed matrix TiO_2-based Nafion™ membranes.

Experimental

Catalyst preparation

The TiO_2 sample was prepared by using titanium(IV) chloride ($TiCl_4$, Fluka 98%) as the starting material. $TiCl_4$ was added under stirring at room temperature to distilled water in the molar ratio $Ti/H_2O = 1 : 60$ and a good dispersion was obtained. After ca. 12 h of stirring, a clear solution was obtained that was boiled for 2 h under agitation. This treatment produced a milky white TiO_2 dispersion that was dried under vacuum at 323 K.

Catalyst characterization

The X-ray diffraction (XRD) pattern of the powder was recorded at room temperature by an Ital Structures APD 2000 powder

diffractometer using CuK-α radiation and a 2θ scan rate of 2° min^{-1}. The crystallite sizes were evaluated by means of the Scherrer equation: $\Phi = K\lambda/(\beta \cos \theta)$, where Φ is the crystallite size, λ is the wavelength of the X-ray radiation (0.154 nm), K is usually taken as 0.89, β is the peak width at half maximum height after subtraction of the equipment broadening, and $\theta = 12.65°$ for TiO$_2$ anatase and $\theta = 13.70°$ for TiO$_2$ rutile. The phase content (%) was calculated using the formula:

$$W_R = \frac{A_R}{(K_A A_A + A_R)}$$

where W_R indicates the content of rutile, A_A and A_R are the integrated intensities of anatase (101) and rutile (110) peaks, respectively, and K_A is a coefficient equal to 0.884.[34]

The specific surface area of the sample was calculated in a Flow Sorb 2300 apparatus (Micromeritics) by using the single-point Brunauer, Emmett and Teller (BET) method. The sample was degassed for 0.5 h at 250 °C prior to the measurement. SEM observations were obtained using a Philips XL30 ESEM microscope, operating at 25 kV on specimens onto which a thin layer of gold had been evaporated.

UV-Vis spectra of the photocatalysts were obtained by diffuse reflectance spectroscopy (DRS) using a Shimadzu UV-2401 PC instrument. BaSO$_4$ was used as a reference sample and the spectra were recorded in the range 200–800 nm. The band gap value was determined by plotting the modified Kubelka–Munk function, $[F(R'_\infty)h\nu]^{1/2}$, versus the energy of the exciting light.

Membrane preparation

Nafion™ (Fig. 1) 5 wt% solution was purchased from Quintech e.K. – Brennstoffzellen Technologie (Germany). Methanol and ethanol were purchased from VWR Prolabo Chemicals (USA). Distilled water was used as a co-solvent for the membranes' preparation. The flat sheet Nafion™ membranes were prepared by using the casting and solvent evaporation technique. Two types of membrane were prepared: a bare Nafion™ membrane (0 wt% of catalyst) and photocatalytic Nafion™ membranes, containing the TiO$_2$ catalyst. In the general procedure adopted,
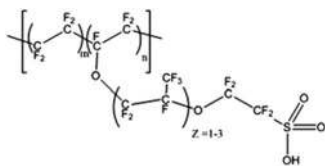

Fig. 1 Nafion™ molecular structure.

the polymer contained in the commercial 5 wt% solution was first recovered by solvent evaporation at 80 °C under magnetic stirring. Then the polymeric solution for membrane preparation was obtained by adding the solvent mixture (MeOH : H$_2$O or EtOH : H$_2$O, 50 : 50 wt%, Table 1) to the recovered polymer under magnetic stirring and at room temperature.

For the preparation of the photocatalytic membranes (membranes 1, 2 and 3), after complete polymer dissolution, the catalyst was added to the obtained solution and the resulting dispersion was left stirring for 1 h more. Then it was sonicated for 30 minutes in order to favour homogenization.

The catalyst and polymer dispersion obtained was then cast in a Petri dish and the solvent was evaporated in a climatic chamber. In the case of blank membrane 4, the same procedure was followed but without catalyst dispersion. For membranes 1 and 4, the temperature of the climatic chamber was 60 ± 4 °C; for membranes 2 and 3 the temperature was 68 ± 4 °C. For all the membrane samples prepared, the relative humidity of the climatic chamber was fixed at 12 ± 5% and the solution volume cast in the Petri dish was selected to give an initial liquid layer thickness of 5 mm.

The membrane surface exposed to air during the evaporation step was indicated as UP whereas the surface in contact with the Petri dish was indicated as DOWN. After solvent evaporation, both types of membranes (photocatalytic and blank) underwent heat treatment at 120 °C for residual solvent removal. Then the flat sheet membranes obtained were detached from the Petri dish with a small amount of water and dried at room temperature. The mean membrane thickness was 75 ± 5 μm.

Membrane characterization

The obtained membranes were characterized by different techniques. The cross-section and surface morphology were observed by scanning electron microscopy (SEM) using a FEI Quanta 200 Philips SEM instrument. Cross-sections were prepared by fracturing the membrane in liquid nitrogen. The samples were "metallized" with graphite. The distribution of heavy elements into the catalytic membranes was observed by using the imaging of a back-scattered electron (BSE) detector in addition to the secondary electron (SE) detector.

A PerkinElmer Spectrum One was utilized for Fourier transform infrared (FT-IR) spectroscopy analyses in attenuated total reflectance (ATR) mode of both UP and DOWN membrane surfaces. The diffuse reflectance UV-Vis spectra were recorded with a PerkinElmer LAMBDA 650 spectrophotometer operating with a 60 mm integrating sphere in a wavelength range between 250 and 800 nm.

Table 1 Membrane preparation conditions

Membrane	1	2	3	4
Solvent in solution, wt%	97.80		97.72	97.83
Polymer in solution, wt%	2.173		2.172	2.174
Catalyst in solution, wt%	0.027		0.109	0
Solvent	MeOH : H$_2$O (50 : 50 wt%)	EtOH : H$_2$O (50 : 50 wt%)	EtOH : H$_2$O (50 : 50 wt%)	MeOH : H$_2$O (50 : 50 wt%)
Catalyst in membrane, wt%	1.2	1.2	5	0

The corresponding reflectance spectra were processed and reported as absorbance spectra in Kubelka–Munk units.

Photocatalytic reaction measurements

The photocatalytic membranes were utilized in CO_2 photoreduction with H_2O as the reducing agent.

A medium–high mercury vapour lamp with emittance from 360 nm (UVA) to 600 nm (Zs lamp, Helios Italquartz, Milan) was used for irradiating the membranes. The runs were carried out by placing the membranes into a flat sheet membrane module equipped with a quartz window, which allowed the UV to irradiate the catalytic membrane surface (active membrane area 19.2 cm^2).

The membrane module was placed in a UV exposure chamber into which a stream of CO_2 was continuously fed by means of a mass flow controller. A water stream was also fed into the chamber by means of an HPLC pump. The $H_2O : CO_2$ feed molar ratio was 5 : 1. The trans-membrane pressure difference was regulated by a back pressure controller and set at 2 bar. Fig. 2 shows a schematic diagram of the experimental apparatus. The membrane reactor consisted mainly of three parts: the feed/retentate chamber, the permeate volume and the catalyst loaded membrane. The two reactor chambers can be considered as lumped parameter systems since no concentration gradient of any chemical species is expected owing to the low conversion of this specific reaction. Inside the membrane, species concentration gradients along the membrane thickness, although very small, are expected owing to permeation and reaction.

The reaction performance was evaluated through MeOH yield and flow rate/TiO$_2$ weight, calculated according to eqn (2) and (3), respectively.

$$\text{MeOH yield} = \frac{\text{MeOH}_{\text{OUT}} \text{ flowrate}}{\text{CO}_2 \text{ feed flowrate}}, \frac{\text{mol min}^{-1}}{\text{mol min}^{-1}} \quad (2)$$

$$\text{MeOH production rate} = \frac{\text{MeOH}_{\text{tot}} \text{ flow rate}}{\text{catalyst mass}}, \frac{\text{mol min}^{-1}}{\text{g}} \quad (3)$$

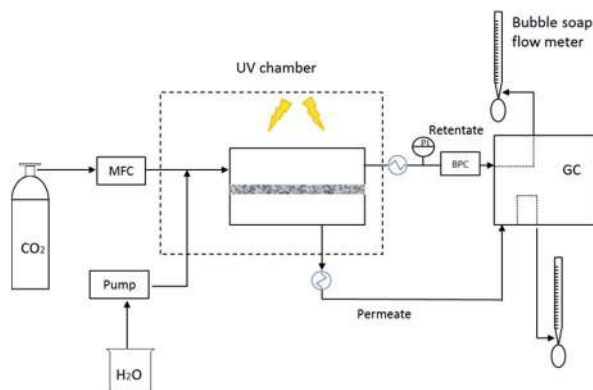Before the photocatalytic experiments with CO_2 as substrate, all of the membranes were subjected to "blank reaction"

Fig. 2 Schematic diagram of the experimental apparatus.

Table 2 Operating conditions for reaction measurements

CO$_2$ (or Ar) flow rate, mL (STP) min^{-1}	20
H$_2$O$_{\text{liquid}}$, mL min^{-1}	0.079
H$_2$O : CO$_2$ (or Ar) molar ratio	5 : 1
Feed pressure–permeate pressure, bar	2
Temperature, °C	45 ± 5

measurements as follows: together with H_2O, an Ar stream was fed into the reaction module instead of CO_2, in continuous mode for 8–12 h under the operating conditions chosen for the catalytic experiments including UV-Vis irradiation (Table 2). The aim of this procedure was to clean the membranes from residuals of solvent and other low molecular weight organics present in the polymer solution that could be released during the reaction test and contaminate the reaction mixture.

Both the retentate and permeate streams exiting the reactor were condensed by means of an ice bath (0 °C). Then the incondensable species in both cases were sent to bubble soap flow meters, in order to evaluate the corresponding flow rates. Moreover, the compositions of these streams were measured by an Agilent Technologies 7890A gas chromatograph with a thermal conductivity detector (TCD; HP-PLOT and Molsieve columns). The condensate components of the retentate and permeate were also periodically sampled and analysed by means of an Agilent Technologies 6890N gas chromatograph with a flame ionization detector (FID; HP-5 column).

Ionic species were determined by ionic chromatography using a Dionex DX 120 instrument equipped with an Ion-Pac AS14 4 mm column (250 mm long, Dionex). The eluent was an aqueous solution of NaHCO$_3$ (8 mM) and Na$_2$CO$_3$ (1 mM). Each membrane was characterized for 15 h, to allow the desired information to be collected. No catalytic or blank measurements were carried out during the night and, thus, 15 h was the maximum time period used. In the case of blank reaction measurements, the liquid samples withdrawn were subjected to total organic carbon (TOC) measurements, by means of a TOC-VCSN Shimadzu analyser, to evaluate the possible presence of organic contaminants in the polymer solution, residual solvent or Nafion™ fractions at low molecular weight. TOC was measured only during blank (no-reaction; Ar + H_2O as feed) tests, confirming the stability under irradiation of the Nafion™ membranes since the obtained values decreased with time.

If not otherwise specified, the membrane was placed into the module exposing the UP surface (i.e. the retentate side) toward the quartz window. Where both sides were exposed, the membrane was placed into the module exposing the retentate side (UP surface) in the first instance and the DOWN (or "Petri side") surface, richer in catalyst, second. Membranes 2 and 3 were only tested with their UP surfaces exposed to reactants and UV light.

Results and discussion

Photocatalyst characterization

The diffraction pattern of the TiO$_2$ sample (Fig. 3a) identifies a mixture of the anatase and rutile polymorphs with a slight degree of crystallinity owing to the low synthesis temperature.

Fig. 4 shows the diffuse reflectance spectra of the prepared sample: the strong absorption in the range 300–380 nm corresponds to the charge transfer process from O 2p to Ti 3d. TiO_2 is an indirect semiconductor so that its band gap energy can be determined from the tangent lines to the plots of the modified Kubelka–Munk function, $[F(R'_\infty)h\nu]^{1/2}$, versus the energy of the exciting light, as shown in the inset of Fig. 4. Some features of the TiO_2 sample are listed in Table 3.

The specific surface area was 54 m^2 g^{-1}, the particle sizes were 12.8 and 2.8 nm for anatase and rutile, respectively, and the band-gap value was 3.00 eV. SEM micrographs indicated that the TiO_2 sample presented irregular shapes and consisted of aggregates of particles whose size was ca. 60 nm (Fig. 3b).

Morphological and chemical characterization of membranes

Fig. 5 shows SEM images of membrane 1. As can be seen from Fig. 5b, many agglomerates of catalyst, appearing as white
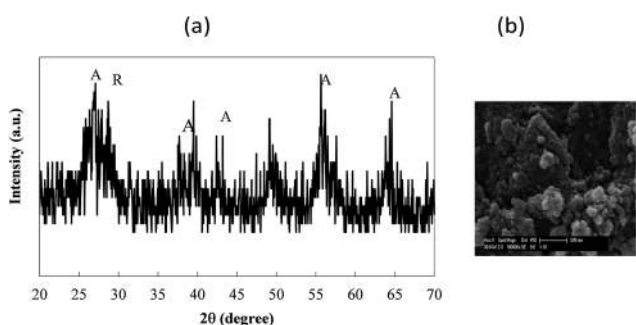

Fig. 3 (a) XRD diffraction pattern of the TiO_2 powder. A = anatase, R = rutile. (b) SEM image of unsupported TiO_2.
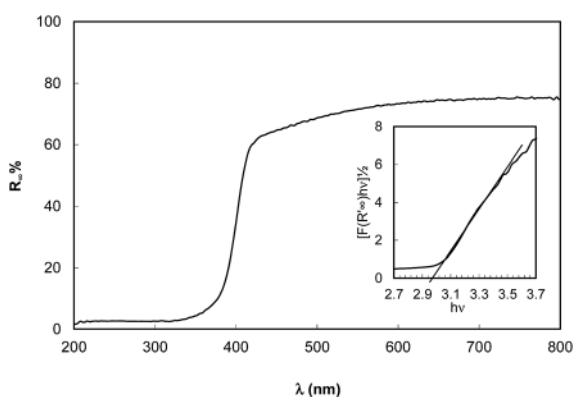

Fig. 4 Diffuse reflectance spectra of the TiO_2 sample. Inset: plot of the square root of the modified Kubelka–Munk function vs. the energy of the absorbed light.

Table 3 Properties of the TiO_2 catalyst

Phases	Phase percentage [%]	Specific surface area [m^2 g^{-1}]	Band gap [eV]	Crystallite size [nm]
Anatase	60	54	3.00	12.8
Rutile	40			2.8

spots, are present throughout the membrane thickness, but are especially concentrated at the bottom surface, and no cavities are visible at this resolution. The presence of a higher concentration of catalyst in the DOWN surface with respect to the UP surface is related to sedimentation phenomena during the $MeOH : H_2O$ solvent evaporation from the polymeric solution. On the contrary, when using the $EtOH : H_2O$ mixture as the solvent in the polymer solution (membranes 2 and 3), a better dispersion of the catalyst in the Nafion™ membrane is observed (Fig. 6) owing to the higher capacity of ethanol to disperse the catalyst in comparison to methanol.

Fig. 6 shows the SEM images of the membrane 2 cross section, both in SE mode and BSE mode (Fig. 6a and b, respectively). The SE SEM image shows that, also in this case, the membrane has no cavities and some small catalyst agglomerates present throughout the membrane thickness. This was confirmed by the BSE image, in which it is also possible to appreciate a relevant improvement of catalyst distribution with respect to membrane 1, which contains the same TiO_2 amount, despite the fact that a residual partial segregation on the DOWN surface can be noticed. Fig. 7 shows BSE images of membrane 3; in particular, Fig. 7b allows many catalyst agglomerates to be observed and again the partial catalyst segregation occurred at the DOWN surface (Fig. 7b and c). This could be due to an excessive amount of TiO_2 with respect to the polymeric matrix, causing its sedimentation during the solvent evaporation step of membrane formation. Also in this case, no visible cavities are present throughout the membrane thickness. The SEM images of the bare polymeric Nafion™ membrane (not shown), confirm that the membrane appears to be characterized by the absence of visible cavities. FT-IR spectroscopy analyses were carried out on both membrane surfaces.
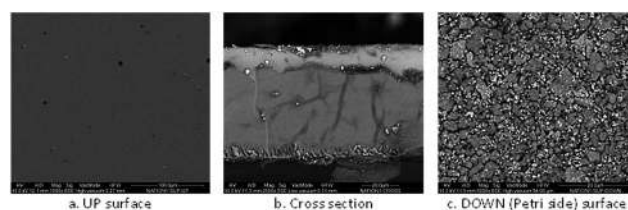

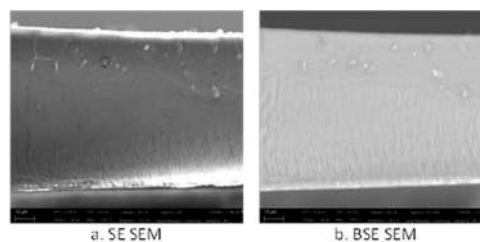Fig. 5 Membrane 1 BSE SEM images (Mag: (a) 1000×; (b) 2500×; (c) 5000×).

Fig. 6 Membrane 2 cross section SEM images (Mag: (a) 2500×; (b) 2500×).
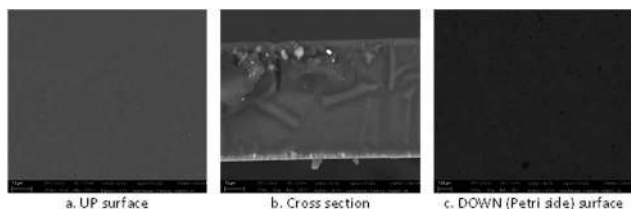
Fig. 7 Membrane 3 BSE SEM images (Mag: (a) 3000×; (b) 3000×; (c) 200×).

To further confirm the integrity of the membranes, permeation measurements with a single gas were also carried out in saturated conditions.

Table 4 summarizes the results for membrane 1 which was dense and highly permeable to CO_2. The presence of water vapour reduced the permeance of all gases; however, CO_2 permeances remained high. Nafion™ membranes are well known in the literature as proton transport[26,27] membranes used in PEMFC (proton exchange membrane fuel cell) with really good chemical stability. Nafion™ has hydrophilic domains favouring membrane hydration that, coupled with the high permeance of CO_2, assures the accessibility of reactants to the whole catalyst dispersed in the membrane.

Fig. 8 shows the spectra relative to the photocatalytic membranes (membranes 1, 2 and 3). All the signals in the range between 970 and 1400 cm^{-1} can be related to the Nafion™ structure. In particular, the bands appearing at 970–983 cm^{-1} are attributed to C–O–C stretching vibrations; the band at $\sim$1060 cm^{-1} can be related to the symmetric stretching of $-SO_3-$. The asymmetric stretching bands of $-SO_3-$ should be found in the range between 1400 and 1100 cm^{-1}, but they are obscured by the more intense bands of $-CF_2$ stretching visible in the spectra.[35] Moreover, it can be seen that OH band intensity is higher for the DOWN surface spectra with respect to the UP surface spectra. This trend could be attributed to the higher

Table 4 CO_2, CH_4 and H_2 permeances of membrane 1 at 25 °C and different RH (relative humidity)

	Permeance, dm^3 (STP) m h^{-1} m^{-2} bar^{-1}		
RH, %	CO_2	CH_4	H_2
0	4.41	6.96	9.19
100	2	1.6	3.4
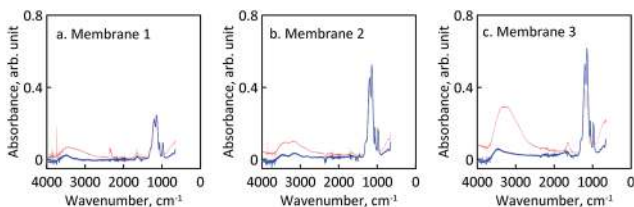
TiO_2 concentration at the DOWN surface (Petri side), as observed in the SEM images (Fig. 5 and 7).

As far as membrane 3 is concerned (Fig. 8c), the signal relating to the OH band has a very different intensity for the UP and DOWN surfaces. This is certainly attributed to a high segregation of the catalyst at the DOWN surface of the membrane, because of the excessive amount of TiO_2. UV-Vis diffuse reflectance spectroscopy was performed on membranes 4 and 1 in order to make a comparison between the bare Nafion™ membrane and that containing the photocatalyst, and to verify the catalyst's structural integrity when embedded inside the polymeric membrane. Membrane 4 gave a flat absorbance spectrum reported in Kubelka–Munk units (Fig. 9b) and obtained by processing the UV-Vis diffuse reflectance spectrum. It shows no absorbance maximum and it is characterized by a constant value of about 5 Kubelka–Munk units, owing to scattering phenomena. The Kubelka–Munk absorbance spectrum relative to membrane 1 (Fig. 9a), containing 1.2 wt% of TiO_2, presents an absorbance maximum of about 13 units in the range 280–300 nm, despite the catalyst segregation. This demonstrates that the catalyst maintains its structural integrity also when embedded inside the Nafion™ matrix, which in turn was proved to be transparent to UV radiation in the wavelength range considered, as the spectrum was recorded when analysing the UP surface.

Photocatalytic reaction measurements

Different measurements were carried out in order to verify the photocatalytic activity of the membranes incorporating the catalyst. In all of them the error bar calculated was below 5%. Firstly, two photocatalytic experiments were performed testing membrane 1 and varying the membrane side exposed to the CO_2/H_2O feed stream and UV irradiation since the SEM and IR characterization had shown that the membrane did not have a symmetric catalyst distribution (Fig. 5b and c and 8a). Table 5 reports the photocatalytic results relating to membrane 1. In the first test performed, the membrane was placed into the module exposing its UP surface to the feed stream and UV radiation whereas, in the second experiment, the DOWN side of the membrane, richer in catalyst, was exposed. In both cases the photocatalytic reaction led to the evolution of CH_3OH as product, in the condensed aqueous phase. No CO or CH_4 were detected (the set up detection limit was 100 ppm).

No significant differences in MeOH yield and MeOH flow rate/TiO_2 weight were observed in the photocatalytic reduction
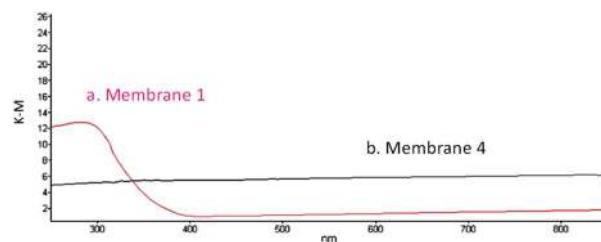

Fig. 8 FT-IR (ATR) spectra of UP membrane surfaces (blue lines) and DOWN membrane surfaces (red lines).

Fig. 9 Absorbance spectra reported in Kubelka–Munk units.

Table 5 Reaction test results relating to membrane 1

	Membrane surface exposed	
	DOWN	UP
Reaction time, min	435	460
MeOH concentration, wt%	1.20×10^{-5}	1.34×10^{-5}
MeOH yield, %	2.07×10^{-5}	2.30×10^{-5}
MeOH flow rate/TiO$_2$ weight, μmol g$_{catalyst}^{-1}$ min^{-1}	0.092	0.10

of CO_2 between the two different exposed surfaces. These results could be attributed to the fact that the Nafion™ polymer matrix is transparent to UV irradiation and therefore not only the superficial layer participates in the reaction, but also the inner layers. It has to be noted that both the CO_2 conversion and the methanol yield have very low values; however, they compare well with literature values. In a second step, membrane 2 was used to test whether the better catalyst distribution inside the bulk of the polymeric matrix (observed with SEM characterization, Fig. 6) could improve the performance of the photocatalytic membrane itself. In this case, the reaction measurements were carried out when just exposing the UP surface as it was observed that the membrane surface exposed to the retentate side does not influence the catalytic performances. One of the main problems relating to the photocatalytic reduction of CO_2 is proving that the products obtained could not be developed from carbon impurities present in the reaction system in the first stage. In order to be sure that the products detected were not due to impurities present in the photocatalytic membrane, the membrane was firstly subjected to "blank" reactions, with UV irradiation of Ar and H_2O streams in the absence of CO_2, according to the operating conditions reported in Table 2. When performing the blank tests, some methanol was detected in the withdrawn samples (Fig. 10A). However, both MeOH wt% (not reported here) and "apparent" MeOH flow rate/TiO$_2$ weight (Fig. 10A) showed a clear decrease with run-time. These results indicate that some organic contaminants, probably due to solvent residuals, were present in the polymeric matrix of the membrane giving the target product. Moreover, the TOC measurements performed on the samples collected confirmed the presence of organics in amounts which decreased with run-time. The corresponding weight percentage was very low (Fig. 10B) but was anyway
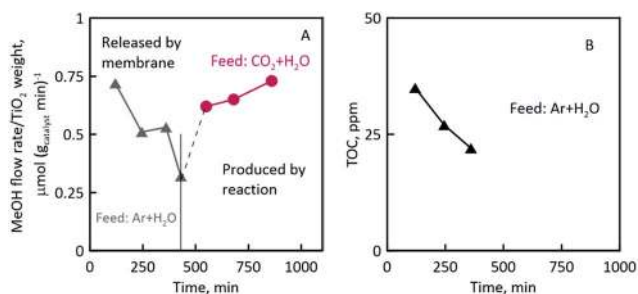
almost two orders of magnitude higher than that of the detected methanol. However, when switching the feeding gas from Ar to CO_2, the real MeOH flow rate/TiO$_2$ weight suddenly increased, reaching a maximum of 0.73 μmol g$_{catalyst}^{-1}$ min^{-1}. The increasing trend of MeOH flow rate/TiO$_2$ weight during the reaction and its decrease in blank tests are indicators of methanol production by CO_2 conversion. In addition, the MeOH flow rate/TiO$_2$ weight value was over 7 times higher than that obtained with membrane 1, confirming that the better catalyst distribution characterizing membrane 2 had a positive effect on the catalytic performance of the membrane itself. Membrane 3 was tested following the previous procedure, feeding Ar until MeOH was not longer measured. Then, CO_2 replaced Ar in the feed and real MeOH production was observed. The MeOH concentration remained almost constant with respect to the test carried out using membrane 2, but the MeOH flow rate/TiO$_2$ weight showed a significant decrease (Fig. 11A), being about 3 times lower. This behaviour could be explained by considering that the increase in the amount of catalyst embedded inside the membrane, caused segregation and this phenomenon could have negatively influenced the performance of the catalytic membrane itself. Indeed, catalyst aggregation could have prevented an effective interaction between TiO$_2$ particles and UV light. Moreover methanol, in the presence of the higher amount of TiO$_2$ in membrane 3, could react. Also in this case, the TOC content in the samples was much higher with respect to MeOH content (Fig. 11B). The same tests were also carried out on membrane 4 (the bare Nafion™), in order to prove that the polymeric matrix does not possess photocatalytic activity by itself.
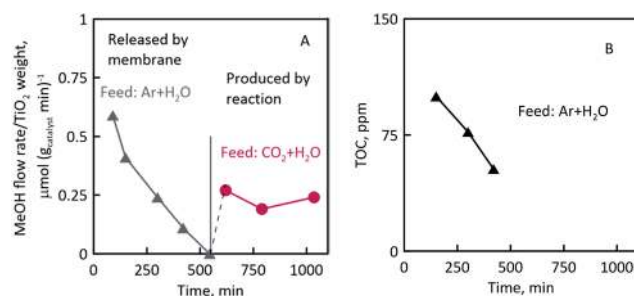

Fig. 11 Photocatalytic results using membrane 3.

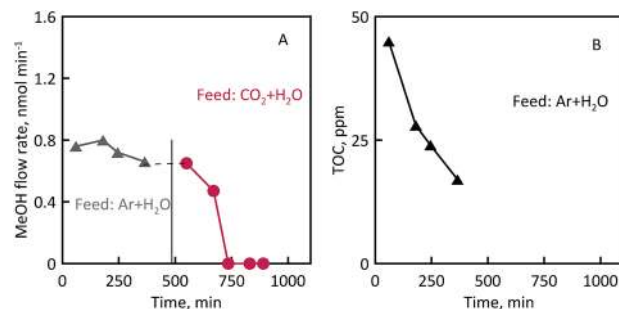**Fig. 10** Photocatalytic results using membrane 2.

Fig. 12 Photocatalytic results using membrane 4.

As can be observed in Fig. 12, both the MeOH flow rate in the samples and the TOC weight percentage reduced with time. In particular, the MeOH content decreased to zero after 750 minutes of irradiation, even after switching the feed from Ar to CO_2.

This path proves that Nafion™ does not possess any catalytic activity and probably, as membrane 4 was prepared by using methanol as the co-solvent, a small residual amount of methanol was released by the membrane during the occurrence of the test. Fig. 13 summarizes the results obtained relative to MeOH flow rate/TiO_2 weight, considering both the quality distribution of the catalyst and its content inside the membrane. At equal TiO_2 amounts (1.2 wt% in the membrane), the better distribution, relating to membrane 2 (labelled in Fig. 13 as "well dispersed") as proved by SEM imaging (Fig. 6), resulted in an increased MeOH flow rate/TiO_2 weight with respect to membrane 1. In the case of membrane 1, the only difference was the partial catalyst deposition (Fig. 5). Increasing the catalyst amount to 5 wt% again produced its partial segregation (Fig. 7) and caused a significant decrease of the photocatalytic performances of the membrane. The visible pink background of membrane 2 highlights its transparency owing
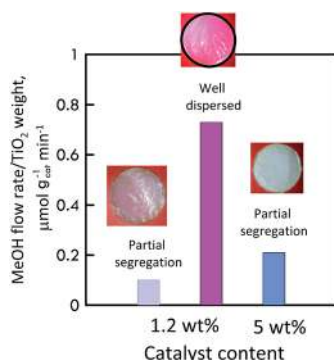
to the good catalyst dispersion. On the contrary, the other membranes did not show similar transparency owing to catalyst segregation.

Consequently, the partial catalyst deposition on the DOWN surfaces of the membranes and the presence of aggregates seem to be crucial parameters for the membrane efficiency, and some strategies should be attempted in order to improve the catalyst distribution at higher content. Such strategies could comprise the reduction of the membrane formation time by accelerating solvent evaporation (e.g. by using higher temperature or gas sweeping), TiO_2 functionalization with surfactants or the use of different polymeric materials.

Nevertheless, even with the current conditions used, the MeOH flow rate/TiO_2 weight was comparable or even much higher than values found in other work presented in the literature (Table 6), although the best results were obtained by Pathak et al.[32] by immobilizing TiO_2 into commercial Nafion™ membranes and by using liquid CO_2 in supercritical conditions as feed.

In the present work a very high MeOH flow rate/TiO_2 weight was obtained under mild operating conditions (atmospheric pressure, room temperature and gaseous CO_2 as feed) and the best results were observed by using membrane 2.
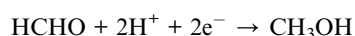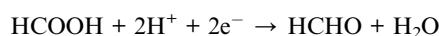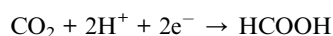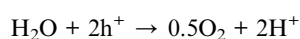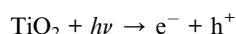
The photocatalytic CO_2 reduction mechanism is very complex and still unclear. Many hypotheses have been advanced on the formation of the various products deriving from CO_2.[36-38] Generally the compounds formed during the gaseous photocatalytic CO_2 reduction are CO and CH_4 (ref. 39 and 40) whilst formic acid, formaldehyde and methanol are mainly observed during liquid phase runs.[41-44]

Published papers[39,43,44] dealing with batch reactors, operating in similar conditions, for CO_2 photo-oxidation over a TiO_2 catalyst showed methane as the main reaction product together with trace formic acid. It is worth noting that, in contrast to that found in most of the literature, in this work neither CH_4 nor CO were detected, methanol being the main product obtained. This can probably be attributed to the synergic effect of the use of membranes inside which the photocatalyst was embedded and

Fig. 13   MeOH flow rate/TiO_2 weight as a function of catalyst content percentage in the polymeric membrane.

Table 6   Comparison of results reported in literature

Catalyst	Reactor configuration	MeOH flow rate/catalyst weight $\mu mol\ (g_{catalyst}\ h)^{-1}$	CH_4, CO, etc. flow rate/catalyst weight $\mu mol\ (g_{catalyst}\ h)^{-1}$	Ref.
TiO_2/Y-zeolite anchored on Vycor glass	Batch	5	8 CH_4	45
Ti-Mesoporous zeolite	Batch	3.5	7.5 CH_4	46
Ti-b(OH) and Ti-b(F)	Batch	5.9	1 CH_4	47
TiO_2 and 2% Cu/TiO_2 in NaOH solution	Batch	0.78 for TiO_2, 19.75 for Cu/TiO_2	—	48
Cu/TiO_2 film supported on optical-fiber	Continuous	0.45	—	49
Cu/TiO_2 and Ag/TiO_2 film supported on optical-fiber	Continuous	4.12	—	5
TiO_2 anatase	Batch	0.075	0.40 CH_4	6
TiO_2 polymorphs	Continuous	—	3.15 CO; 2.13 CH_4	50
TiO_2 polymorphs	Continuous	—	2.1 CO	11
Phthalocyanines/TiO_2	Batch	—	26 HCOOH	43
TiO_2 nanoparticles in porous cavities of commercial Nafion™ membranes	Continuous	56 (using supercritical CO_2 as feed)	38 HCOOH, 6 CH_3COOH	32
TiO_2 nanoparticles in Nafion™ membrane	Continuous	45 (membrane 2), 12.6 (membrane 3)	Traces of HCOOH (membrane 2)	This work

a continuous flow mode reactor to carry out the reaction of CO_2 and H_2O. Actually, avoiding the use of a batch reactor results in the substrate undergoing a lower degree of reduction as fresh CO_2 is continuously fed into the system and the produced methanol is continuously removed from the catalytic sites, reducing the possibility of over oxidation phenomena.[39] Ion chromatography analyses, performed on selected samples, revealed that trace amounts of formic acid were formed in the presence of membrane 2. Methanol formation is a multi-electronic process which, in the presence of TiO_2 and H_2O, can occur in different stages according to the reported reactions below (adapted from literature data):

$$TiO_2 + h\nu \rightarrow e^- + h^+$$

$$H_2O + 2h^+ \rightarrow 0.5O_2 + 2H^+$$

$$CO_2 + 2H^+ + 2e^- \rightarrow HCOOH$$

$$HCOOH + 2H^+ + 2e^- \rightarrow HCHO + H_2O$$

$$HCHO + 2H^+ + 2e^- \rightarrow CH_3OH$$

In our system formic acid and formaldehydes were not detected, or were present in low amounts (in the case of HCOOH with membrane 2), which can be explained by the fast reaction rate of these compounds to form methanol or by direct methanol formation. Moreover, the continuous removal of methanol from the reaction volume avoids its oxidation.

As an overall consideration it can be seen that the yields of methanol and thus CO_2 conversion are very low, if evaluated as absolute values, even if they are among the best reported in the literature. It has to be considered that this process is at a very early stage of development and it needs more effort to make it profitable. However, it remains highly promising and attractive, as it has the great advantage of being completely green, using CO_2 and water as reactants, exploiting sunlight as the energy source and producing liquid fuels.

Conclusions

In this work, the photocatalytic conversion of CO_2 to methanol was carried out in a continuous membrane reactor with a TiO_2-based membrane irradiated by UV light.

Various photocatalytic membranes were prepared embedding the TiO_2 catalyst inside a polymeric Nafion™ matrix. A good distribution of catalyst was achieved by choosing an appropriate co-solvent for the preparation of the polymeric solution (e.g. ethanol) at a chosen catalyst concentration of 1.2 wt%.

By using membrane 2, which displayed the best TiO_2 distribution, neither CH_4 nor CO formation were observed whereas a MeOH flow rate/TiO_2 weight of 45 μmol $(g_{catalyst}\ h)^{-1}$ was obtained under mild experimental conditions. It is our understanding that such a value is a relevant advance over values reported to date in the existing literature as it is higher than most of the data, without using supercritical CO_2.

Moreover, it was observed that the catalytic performances were strictly related to the membrane preparation process; the higher MeOH flow rate/TiO_2 weight was achieved by using the photocatalytic membrane with the best catalyst distribution (membrane 2) rather than that with the highest catalyst content (membrane 3). Comparing the results to those of the bare Nafion™ membrane, it was demonstrated that the polymeric matrix does not possess any photocatalytic activity by itself and, thus, the methanol production has to be attributed to the presence of the catalyst dispersed in the Nafion™ matrix.

The present work demonstrates that photocatalytic Nafion™ membranes offer a wide range of potential improvements and could be promising candidates for the development of an advanced route for CO_2 conversion to methanol.

Acknowledgements

References

1 https://co2.earth/global-co2-emissions, Last Access: 27/01/2016.

2 A. Brunetti, F. Scura, G. Barbieri and E. Drioli, J. Membr. Sci., 2010, 359, 115–125, DOI: 10.1016/j.memsci.2009.11.040.

3 S. C. Roy, O. K. Varghese, M. Paulose and C. A. Grimes, ACS Nano, 2010, 4, 1259–1278.

4 A. Dhakshinamoorthy, S. Navalon, A. Corma and H. Garcia, Energy Environ. Sci., 2012, 5, 9217–9233.

5 J. C. S. Wu, Catal. Surv. Asia, 2009, 13, 30–40.

6 K. Kočí, L. Obalová, L. Matějová, D. Plachá, Z. Lacný, J. Jirkovský and O. Ŝolcová, Appl. Catal., B, 2009, 89, 494–502.

7 T. Inoue, A. Fujishima, S. Konishi and K. Honda, Nature, 1979, 277, 637–640.

8 J. C. Hemminger, R. Carr and G. A. Somorjai, Chem. Phys. Lett., 1978, 57, 100–108.

9 S. Das and W. M. A. Wan Daud, RSC Adv., 2014, 4, 20856–20893.

10 K. Kočí, L. Obalová and Z. Lacný, Chem. Pap., 2008, 62, 1–9.

11 H. Zhao, L. Liu, J. M. Andino and Y. Li, J. Mater. Chem. A, 2013, 1, 8209–8216.

12 R. Molinari, M. Mungari, E. Drioli, A. Di Paola, V. Loddo, L. Palmisano and M. Schiavello, Catal. Today, 2000, 55, 71–78.

13 R. Molinari, L. Palmisano, E. Drioli and M. Schiavello, J. Membr. Sci., 2002, 206, 399–415.

14 H. Choi, E. Stathatos and D. D. Dionysiou, Desalination, 2007, 202, 199–206.

15 H. Choi, A. C. Sofranko and D. D. Dionysiou, Adv. Funct. Mater., 2006, 16, 1067–1074.

16 A. Pandikumar, S. Murugesan and R. Ramaraj, ACS Appl. Mater. Interfaces, 2010, 2, 1912–1917.

17 C. Pandiyarajan, A. Pandikumar and R. Ramaraj, *Nanotechnology*, 2013, **24**, 435401.

18 A. Pandikumar, S. Manonmari and R. Ramaraj, *Catal.: Sci. Technol.*, 2012, **2**, 345–353.

19 A. Pandikumar and R. Ramaraj, *J. Hazard. Mater.*, 2012, **203–204**, 244–250.

20 I. R. Bellobono, B. Barni and F. Gianturco, *J. Membr. Sci.*, 1995, **102**, 139–147.

21 A. Barni, A. Cavicchioli, E. Riva, L. Zanoni, F. Bignoli, I. R. Bellobono, F. Gianturco, A. De Giorgi, H. Muntau, L. Montanarella, S. Facchetti and L. Castellano, *Chemosphere*, 1995, **30**(10), 1861–1874.

22 H. Dzinun, M. H. D. Othman, A. F. Ismail, M. H. Puteh, M. A. Rahman and J. Jaafar, *Chem. Eng. J.*, 2015, **269**, 255–261.

23 S. Leong, A. Razmjou, K. Wang, K. Hapgood and X. Zhang, *J. Membr. Sci.*, 2014, **472**, 167–184.

24 P. Liu, J. Bandara, Y. Lin, D. Elgin, L. F. Allard and Y. P. Sun, *Langmuir*, 2002, **18**, 10398–10401.

25 Y. P. Sun, P. Atorngitjawat, Y. Lin, P. Liu, P. Pathak, J. Bandara, D. Elgin and M. Zhang, *J. Membr. Sci.*, 2004, **245**, 211–217.

26 H. Miyoshi, S. Nippa, H. Uchida, H. Mori and H. Yoneyama, *Bull. Chem. Soc. Jpn.*, 1990, **63**(12), 3380–3384.

27 K. A. Mauritz and R. B. Moore, *Chem. Rev.*, 2004, **104**, 4535–4585.

28 E. Drioli and E. Fontananova, *Annu. Rev. Chem. Biomol. Eng.*, 2012, **3**, 395–420.

29 F. R. F. Fan, H. Y. Liu and A. J. Bard, *J. Phys. Chem.*, 1985, **89**, 4418–4420.

30 A. Yaron and L. Arcan, *Thin Solid Films*, 1990, **185**, 181–188.

31 J. Premkumar and R. Ramaraj, *J. Photochem. Photobiol., A*, 1997, **110**, 53–58.

32 P. Pathak, M. J. Meziani, Y. Li, L. T. Cureton and Y. P. Sun, *Chem. Commun.*, 2004, 1234–1235.

33 P. Pathak, M. J. Meziani, L. Castillo and Y. P. Sun, *Green Chem.*, 2005, **7**, 667–670.

34 H. Zhang and J. F. Banfield, *J. Phys. Chem. B*, 2000, **104**, 3481–3487.

35 Z. Liang, W. Chen, J. Liu, S. Wang, Z. Zhoua, W. Li, G. Suna and Q. Xin, *J. Membr. Sci.*, 2004, **233**, 39–44.

36 G. R. Dey, *J. Nat. Gas Chem.*, 2007, **16**, 217–226.

37 S. N. Habisreutinger, L. Schmidt-Mende and J. K. Stolarczyk, *Angew. Chem., Int. Ed.*, 2013, **52**, 2–39.

38 Y. Izumi, *Coord. Chem. Rev.*, 2013, **257**, 171–186.

39 M. Bellardita, A. Di Paola, E. García-López, V. Loddo, G. Marcì and L. Palmisano, *Curr. Org. Chem.*, 2013, **17**, 2440–2448.

40 W. Lin, H. Han and H. Frei, *J. Phys. Chem. B*, 2004, **108**, 18269–18273.

41 G. Qin, Y. Zhang, X. Ke, X. Tong, Z. Sun, M. Liang and S. Xue, *Appl. Catal., B*, 2013, **129**, 599–605.

42 Slamet, H. W. Nasution, E. Purnama, S. Kosela and J. Gunlazuardi, *Catal. Commun.*, 2005, **6**, 313–319.

43 G. Mele, C. Annese, A. De Riccardis, C. Fusco, L. Palmisano, G. Vasapollo and L. D'Accolti, *Appl. Catal., A*, 2014, **481**, 169–172.

44 G. Mele, C. Annese, L. D'Accolti, A. De Riccardis, C. Fusco, L. Palmisano, A. Scarlino and G. Vasapollo, *Molecules*, 2015, **20**, 396–415.

45 M. Anpo, H. Yamashita, Y. Ichihashi, Y. Fujii and M. Honda, *J. Phys. Chem.*, 1997, **101**, 2632–2636.

46 H. Yamashita, Y. Fujii, Y. Ichihashi, S. G. Zhang, K. Ikeue, D. R. Park, K. Koyano, T. Tatsumi and M. Anpo, *Catal. Today*, 1998, **45**, 221–227.

47 K. Ikeue, H. Yamashita and M. Anpo, *J. Phys. Chem. B*, 2001, **105**, 8350–8355.

48 I.-H. Tseng, W. C. Chang and J. C. S. Wu, *Appl. Catal., B*, 2002, **37**, 37–48.

49 J. C. S. Wu, H. M. Lin and C. L. Lai, *Appl. Catal., A*, 2005, **296**, 194–200.

50 L. Liu, H. Zhao, J. M. Andino and Y. Li, *ACS Catal.*, 2012, **2**, 1817–1828.